Journal of Electroanalytical Chemistry 921 (2022) 116676

Contents lists available at ScienceDirect

Journal of Electroanalytical Chemistry

journal homepage: www.elsevier.com/locate/jelechem

An effective metal-organic framework-based electrochemical non-enzymatic glucose sensor

A.D. Daud [a], H.N. Lim [a,b,*], I. Ibrahim [a,*], N.A. Endot [b], N.S.K. Gowthaman [a], Z.T. Jiang [c], Kyle E. Cordova [a,b,d]

[a] Foundry of Reticular Materials for Sustainability (FORMS) Laboratory, Institute of Nanoscience and Nanotechnology (ION2), Universiti Putra Malaysia, 43400 UPM Serdang, Selangor, Malaysia
[b] Department of Chemistry, Faculty of Science, University Putra Malaysia, 43400 UPM Serdang, Selangor, Malaysia
[c] Surface Analysis and Materials Engineering Research Group, College of Science, Health, Engineering and Education, Murdoch University, Murdoch, WA 6150, Australia
[d] Materials Discovery Research Unit, Advanced Research Centre, Royal Scientific Society, Amman 11941, Jordan

ARTICLE INFO

Keywords:
Metal-organic frameworks
Chemosensor
Glucose
Electrochemical activity
Non-enzymatic sensing
Reticular chemistry

ABSTRACT

Herein, we report a non-enzymatic glucose sensor based on a metal-organic framework (MOF) as alternative approach for long-term glucose monitoring. Specifically, nickel-based MOFs were solvothermally synthesized using either 2-amino-1,4-benzenedicarboxylic acid (BDC-NH_2) or 2-hydroxy-1,4-benzenedicarboxylic acid (H_2BDC-OH), both of which were characterized by different physicochemical techniques. The electrochemical performance of both electrodes towards glucose sensing was investigated and Ni-BDC-NH_2 exhibited a significantly better electrocatalytic behaviour towards oxidation of glucose than bare Ni-BDC or Ni-BDC-OH in an alkaline media. This was attributed to a favourable multi-layered sheet-like structure that allowed diffusion for entrapment of glucose and the incorporation of –NH_2 functional groups attached to the BDC linker which, were responsible for electrochemical adsorption of glucose molecules. Ni-BDC-NH_2 displayed a lower detection limit (3.82 μM), higher stability (>180 days), and remarkable sensitivity (308 μA mM^{-1} cm^{-2}). Additionally, a molecular sieve effect for Ni-BDC-NH_2 led to a noteworthy anti-interference ability and the sensor displays a fast response time of 5.4 s towards glucose detection. These results indicate that the as-synthesized non-enzymatic glucose sensor operates with a longer lifetime and is viable for use as an intensive monitoring system.

1. Introduction

High blood glucose may lead to an acute diseases such as diabetes, obesity and hypertension, which subsequently results in significant financial burden associated with reduced quality of life [1]. As a consequence, there is a high demand for cost-effective, rapid, and reliable quantitative determination of glucose concentration that leads to continuing industry interest in developing new sensors for clinical diagnostics, food industry and biotechnology. To date, commercially available glucose biosensors are predominantly based on catalytic activity of an immobilized enzyme, which offers a high sensitivity and satisfactory selectivity. However, enzyme-based glucose sensors mostly experience the problems of instability and are expensive to produce associated with sophisticated immobilization procedures, which are badly affected by the surrounding circumstance [2]. Therefore, the advancement of electrochemical non-enzymatic glucose sensors that commonly rely on the current response of directly oxidizing glucose molecules is crucial and considered the most effectual and favourable approach for glucose detection.

Metal-organic frameworks (MOFs), composed of metal clusters connected by organic linkers, are an attractive porous material with exceptional specific surface area, tuneable pore size, and abundant active sites that can be exploited as catalysts for glucose detection [3,4]. The distinctive framework and porous structure of MOFs created an abundance of exposure for a functional element that may perform as catalytic centres for glucose sensing. Ample exposed active sites lead to interesting catalytic properties in MOF, including exceptional sensitivity and lowest limit of detection. More significantly, the molecular sieve effect of MOF (due to compatible pore sizes of the MOF and glucose molecules) during sensing has overcome the problem of poor selectivity of non-enzymatic catalyst [5]. Moreover, various strategies have been employed to tune the size, morphology and sensitivity of MOFs towards glucose detection, including the use of functionalized linkers bearing –NH_2, –COOH and –SO_3H functional groups [6]. This

* Corresponding authors at: Foundry of Reticular Materials for Sustainability (FORMS) Laboratory, Institute of Nanoscience and Nanotechnology (ION2), Universiti Putra Malaysia, 43400 UPM Serdang, Selangor, Malaysia (H.N. Lim).
E-mail addresses: hongngee@upm.edu.my (H.N. Lim), izwaharyanie@upm.edu.my (I. Ibrahim).

https://doi.org/10.1016/j.jelechem.2022.116676
Received 12 May 2022; Received in revised form 26 July 2022; Accepted 3 August 2022
Available online 06 August 2022

approach is not only able to control the surface morphology, but impart the conductivity in MOFs due to the highly conjugated and delocalized π-bond in the linker, as well as to enhance the electrochemical adsorption of the glucose molecule. Hence, this architecture facilitates the electron transport and promotes excellent conductivity and electrochemical adsorption of the system [7].

Accordingly, we fabricated 3D π-conjugated MOFs composed of nickel and a functionalized linker [2-amino-1,4-benzenedicarboxylic acid (BDC-NH_2) or 2-hydroxy-1,4-benzenedicarboxylic acid (H_2BDC-OH)] via a simple solvothermal approach. The as-synthesized MOFs were then drop-casted on a glassy carbon electrode (GCE) and acted as working electrodes for a non-enzymatic glucose sensor. The MOF materials were examined as glucose sensors using a range of physicochemical techniques to evaluate their catalytic activity. Amperometry studies indicated that Ni-BDC-NH_2 MOF exhibited excellent electrocatalytic activity towards glucose oxidation with a lower detection limit, higher sensitivity and remarkable stability. This was correlated to the numerous electroactive sites and favourable porous structure, both of which not only facilitate a close interaction between glucose and the active sites throughout the pores and channels in MOF, but also greatly enhance conductivity through the conjugated π-bond in the linker. Ultimately, the acquired results suggest high potential for the proposed sensor's use in long-term glucose monitoring.

2. Experimental section

2.1. Materials

Chemical reagents including nickel(II) nitrate hexahydrate (Ni$(NO_3)_2{\cdot}6H_2O$, ≥97.0 % purity), 1,4-benzenedicarboxylic acid (BDC, 98 % purity), 2-amino-1,4-benzenedicarboxylic acid (BDC-NH_2, 99 % purity), 2-hydroxy-1,4-benzenedicarboxylic acid (H_2BDC-OH, 98 % purity), *N*,*N*′-dimethylformamide (DMF, 99.8 % purity), dichloromethane (DCM, ≥99.8 % purity), dopamine hydrochloride (DA, 98 % purity), and *D*-(+)-glucose (Glu, ≥99.5 % purity) were purchased from Sigma-Aldrich. Ethanol (EtOH, 95 % purity) was purchased from R&M Chemicals, Malaysia. Uric acid (UA, ≥99 % purity) and L-ascorbic acid (AA, 99 % purity) of analytical grade were obtained from Merck, USA. All reagents were used as received without further purification. During the experiment, Milli-Q deionised water with a resistivity of 18.2 MΩ cm^{-1} was used. All analyses were performed at room temperature.

2.2. Synthesis of Ni-BDC, Ni-BDC-NH_2, and Ni-BDC-OH MOF

Ni$(NO_3)_2{\cdot}6H_2O$ (0.44 g, 1.5 mmol) and BDC (0.17 g, 1.0 mmol) were dissolved in 20 mL of DMF under magnetic stirring for 30 min. A clear, green solution was obtained and transferred into five borosilicate glass tubes (4 mL each in 10 mL glass tubes). The glass tubes were subsequently sealed under ambient atmosphere and temperature and placed in an isothermal oven. The solution was heated at 120 °C for 6 h to yield green powder of Ni-BDC MOF. After cooling to room temperature, the products were washed with 10 mL of DMF (6 times) and immersed in DMF for 3 d. The products were solvent exchanged with 10 mL of DCM (6 times) and immersed in DCM for 2 d. Ni-BDC was heated at 100 °C for 1 h to obtained an activated product. Ni-BDC-NH_2 and Ni-BDC-OH were synthesised using a similar approach, but by replacing BDC with BDC-NH_2 or H_2BDC-OH linkers, respectively.

2.3. Material characterization

The morphologies of the samples were characterised using field emission scanning electron microscope (FE-SEM; FEI Quanta SEM Model 400 F, USA), and energy-dispersive X-ray spectroscopy (EDX: Bruker Nano, Germany). Fourier transform infrared (FT-IR) spectroscopy analysis was measured on a Perkin Elmer, USA FT-IR spectrometer with the tested wavenumber range being from 400 to 4000 cm^{-1}. The crystalline phase purity of the as-synthesized MOFs was analysed using X-ray diffraction (XRD) on a PW 3040/60 MPD X'pert Pro PANlytical, Netherland with Cu Kα radiation (λ = 1.5418 Å) over a 2θ range of 2 to 40°.

2.4. Fabrication of modified electrodes for glucose sensing

Saturated Ag/AgCl electrode, Pt wire and glassy carbon electrode (GCE; 2 mm diameter) was used as reference, counter, and working electrodes, respectively. The surface of the GCE was polished to create a mirror finish with 0.35 μm of alumina slurry on the polishing rag. The electrode was then sonicated for approximately 2 min with absolute ethanol and distilled water, and eventually dried under ambient temperature. The as-synthesized MOFs were deposited on the GCE via drop-casting method. Afterward, 5 μL of an aqueous solution of Nafion (0.5 wt%) was casted on the modified electrode and dried at room temperature. The modified electrode was then positioned in a 0.1 M NaOH electrolyte which was purged with N_2 gas to remove dissolved oxygen and reduce the interference during the analysis. The cyclic voltammogram (CV) measurements were undertaken at a scan rate of 50 mV s^{-1} over a potential window of 0–0.7 V. CV was conducted for at least 10 scans until a reproducible CV curve was acquired. Finally, the modified electrode was ready to use for subsequent experiments.

2.5. Electrochemical characterizations

The characterization of electrodes was carried out by CV in 0.1 M NaOH with a scan rate of 50 mV s^{-1} over a potential range from 0 to 0.7 V. Chronoamperometry (CA) measurements were evaluated in galvanostatic mode using an over limiting current of 0.55 V. Both CV and CA were measured and analysed with a potentiostat (Metrohm, Autolab μSTAT 8000P) integrated with a frequency response analyzer (FRA32M). Electrochemical impedance spectroscopy (EIS) measurements with a frequency range of 0.01 Hz–100 kHz were executed on a Princeton Applied Research VersaSTAT 4 workstation. All electrochemical characterization was carried out in 10 mL of a single compartment electrochemical cell, which stationed all three electrodes. A Metrohm pH metre (model 827) was used for all pH measurements.

3. Results and discussion

3.1. Physicochemical characterization of MOFs

Nickel-based MOFs were synthesized under solvothermal reaction conditions by dissolving Ni$(NO_3)_2{\cdot}6H_2O$ with BDC, BDC-NH_2 and H_2BDC-OH organic linkers, respectively in DMF and the solution was transferred into a borosilicate glass tube. The glass tube was sealed under ambient atmosphere and placed in an oven at 120 °C for 6 h. Activated powder of each Ni-MOF with different color intensities (apple green to greenish-brown color) were obtained depending on the organic linkers used (Supplementary Information, Fig. S1). Different functionalized linkers containing –NH_2 and –OH functional groups in the synthesis of the Ni-MOFs were employed for the opportunity of tuning the morphology and the conductivity of the materials. Additionally, this will provide ample active sites for glucose catalysis with the highly conjugated and delocalized π-bond in the linkers being used to further improve the detection sensitivity.

The crystalline structure and phase purity of the synthesized MOFs were analysed by XRD (Fig. 1A). The major diffraction peaks present for XRD of experimental Ni-BDC, Ni-BDC-NH_2 and Ni-BDC-OH were in good agreement with the simulated Ni-BDC (Cambridge Crystallographic Data Center (CCDC) No. 638866) [8], deducing that the

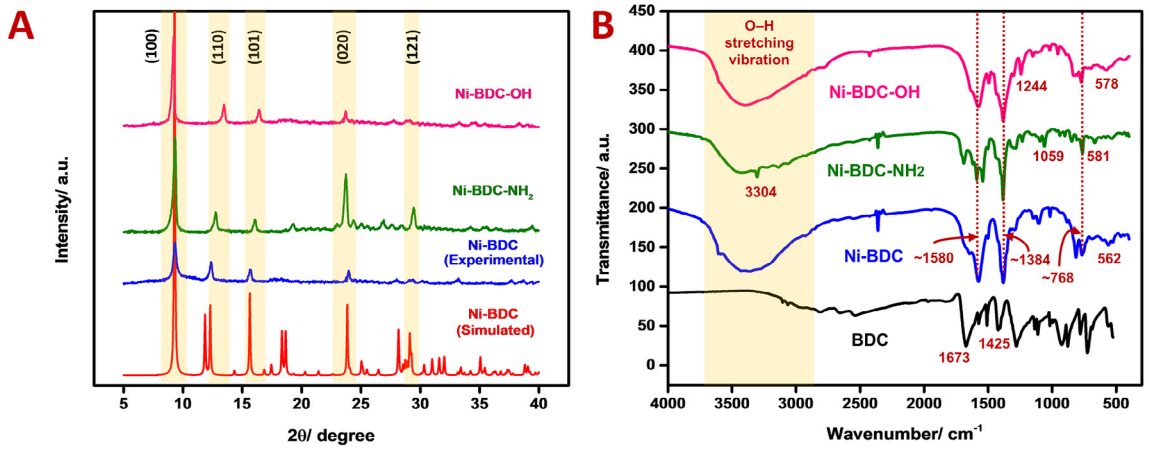

Fig. 1. (A) XRD of Ni-BDC (simulated), Ni-BDC (experimental), Ni-BDC-NH_2 and Ni-BDC-OH MOF and (B) FT-IR spectra of BDC, Ni-BDC, Ni-BDC-NH_2 and Ni-BDC-OH MOF.

amino- and hydroxyl-functionalization of BDC linker molecule had no notable impact on the crystal structure of Ni-BDC. The XRD pattern of all the MOFs samples exhibit a major diffraction peak at average 2θ of 8.8°, 12.9°, 16.1°, 23.9° and 29.4° attributed to the (100), (110), (101), (020) and (121) Miller planes, respectively, indicating that all the compounds have very similar XRD patterns and hence confirming the retained 3D structure upon linker functionalization [9]. Peak broadening and lower signal intensity in the XRD spectra of Ni-BDC (experimental) and Ni-BDC-OH at the Miller planes of (020) was detected, which makes the peak difficult to discern. Moreover, a minor shift on the position and width as well as intensity of few peaks was observed due to the existence of solvent which will influence the stability of the crystallites. The schematic illustration on the structure of simulated Ni-BDC reported by Carton et al. [8] is depicted in the Supplementary Information, Fig. S2.

FT-IR spectroscopic characterization was used to examine the integration of functional groups within the as-synthesized MOFs structure. From Fig. 1B, two intense absorption bands at 1673 and 1425 cm^{-1} were identified as characteristic of the linker BDC. These represent the asymmetric and symmetric carboxyl ($–COO^-$) stretching vibrations. However, these bands were absent in the spectra for Ni-BDC, Ni-BDC-NH_2 and Ni-BDC-OH, therewith verify the coordination of the linkers with a metal centre of Ni^{2+} [10,11]. Shifting of the absorption bands at ca. 1580 and 1384 cm^{-1} for Ni-BDC, Ni-BDC-NH_2 and Ni-BDC-OH corresponded to the asymmetric and symmetric $–COO^-$ stretching vibrations of the linker coordinated to the metal centre [10]. Further, Ni-BDC, Ni-BDC-NH_2 and Ni-BDC-OH spectra have a broad band at 3700–2700 cm^{-1}, attributed to O—H stretching vibration in water molecules, indicating the binding of O—H to the open metal sites [12]. Furthermore, bands at 3304 and 1059 cm^{-1} were observed in the Ni-BDC-NH_2 that were attributed to stretching vibrations of N—H and C—N, respectively. The FT-IR spectrum of Ni-BDC-OH revealed a peak at 1244 cm^{-1}, indicating the C–OH stretching vibration of BDC-OH. The located absorption bands at ~768 cm^{-1} were due to the aromatic rings in the organic linkers. Moreover, the appearance of Ni–O peaks at 562, 581 and 578 cm^{-1} correspond to the present of the metal–oxo bond with the Ni atoms and the carboxylate groups of the BDC, BDC-NH_2 and H_2BDC-OH linker, respectively. These results imply the successful coordination of the metals with each of the linkers.

Morphology and microstructural characteristic of the as-synthesized MOFs have been investigated by FE-SEM (Supplementary Information, Fig. S3A). The morphology of Ni-BDC can be described as randomly orientated thick plate shaped particles with uneven edges. However, the morphology of the MOF varies depending on the linker used. Upon functionalization of BDC linker with the $–NH_2$ functional group, Ni-BDC-NH_2 MOF displayed hundreds of micro-scale three-dimensional sheets, which were loosely stacked together forming ordered lamellar structures (Supplementary Information, Fig. S3B). The detailed morphology of Ni-BDC-NH_2 was supported by the high-magnification image, which revealed a hierarchical multi-layered sheet-like structure with the average thickness of ~0.092 μm (Supplementary Information, Fig. S3B). Furthermore, it was observed from the images that the micro-sheets form a great deal of gaps between the layers, hence creating a multidimensional porous structure. This architecture gives plenty exposed surfaces which can provide a significant number of $–NH_2$ active sites for electrocatalytic oxidation of glucose molecules and accelerate the diffusion velocity of the guest molecules [3]. Functionalization of Ni-BDC with hydroxyl group show large thick plates assemble and densely stack together forming flat bricks (Supplementary Information, Fig. S3C). Some part on the Ni-BDC-OH morphology was observed to have the similar structure as Ni-BDC MOF. The EDX analysis demonstrated that the MOFs were composed of C, O and Ni for the Ni-BDC and Ni-BDC-OH MOFs, and additional of N atom was depicted on the spectrum of Ni-BDC-NH_2. The EDX measurement for all three MOFs clearly confirms the presence and distribution of the atoms in their structure.

3.2. Electrochemical performance of modified electrodes

Fig. 2A show the CV profiles of bare GCE, Ni-BDC, Ni-BDC-NH_2 and Ni-BDC-OH modified GCE electrodes performed in 0.1 M NaOH at a scan rate of 50 mV s^{-1}. The CV curves of Ni-BDC, Ni-BDC-NH_2 and Ni-BDC-OH consisted of redox peaks. The current outputs at the redox peaks were profound for Ni-BDC-NH_2 curve as compared to other modified electrodes. The results show that the interaction between BDC-NH_2 and Ni^{2+} forming Ni-BDC-NH_2 has facilitated the transfer of electron from BDC-NH_2 to Ni^{2+} [13]. Further, the Ni-BDC-NH_2 having benzene-derived linkers that possess adjacent substituted N donor atoms form a highly conjugated and delocalized π-bond in the linker, which greatly amplified its redox properties [14].

To study the effect of pH on the electrocatalytic glucose oxidation of the synthesized Ni-BDC-NH_2 MOF, current-potential responses at different pH (in 1 mM glucose) was investigated to compare their anodic peak current value. A clear histogram for the anodic peak current was depicted in the Supplementary Information, Fig. S4. It was evident that the anodic peak current increases upon increasing pH from 6 to 14. This is expected as, metal-based glucose sensor work in high pH ($pH \geq 11$) because it requires the presence of hydroxide ions to oxidize target glucose molecules [15]. When the pH reached 14, a slight

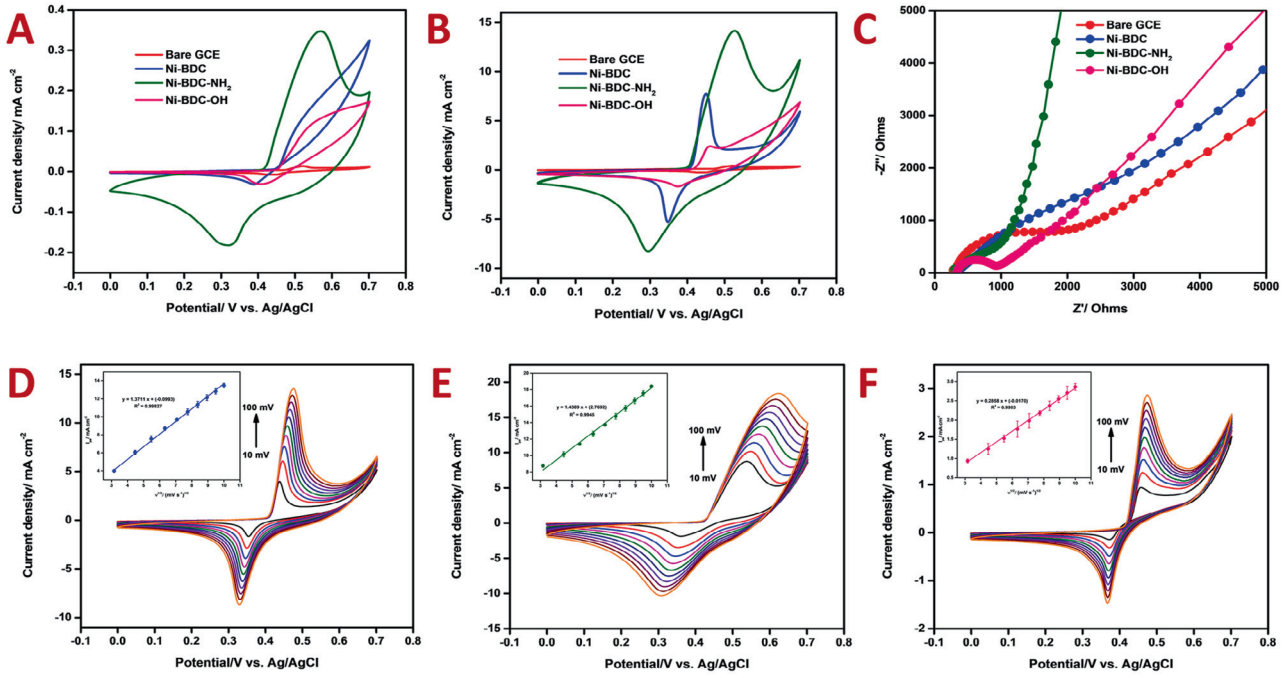

Fig. 2. CV profiles of bare GCE, Ni-BDC, Ni-BDC-NH_2 and Ni-BDC-OH electrodes in the (A) absence and (B) presence of 1 mM glucose at a scan rate of 50 mV s^{-1}. (C) Nyquist plot of bare GCE, Ni-BDC, Ni-BDC-NH_2 and Ni-BDC-OH in 1 mM $[Fe(CN)_6]^{3-/4-}$ with 0.1 M KCl as the supporting electrolyte and 1 mM glucose. CV profiles at different scan rates from 10 to 100 mV s^{-1} in 0.1 M NaOH with 1 mM glucose for (D) Ni-BDC, (E) Ni-BDC-NH_2 and (F) Ni-BDC-OH electrode. Inset: anodic current against $\nu^{1/2}$ (n = 3).

decrease in anodic peak current was observed owing to the limited loading of active materials on the electrode. Therefore, pH = 13 was selected as an optimal pH condition in all further studies for electrochemical non-enzymatic glucose detection.

Fig. 2B displays the CV of Ni-BDC, Ni-BDC-NH_2 and Ni-BDC-OH electrodes in 0.1 M NaOH electrolyte containing 1 mM glucose (pH = 13) at a scan rate of 50 mV s^{-1}. Based on the CV profiles shows in Fig. 2B, it was confirmed that deposition of MOFs (Ni-BDC, Ni-BDC-NH_2 and Ni-BDC-OH) on the GCE increases the oxidation current compared to the bare GCE (I_{GCE} = 0.43 mA cm^{-2} at 0.52 V vs $I_{Ni\text{-}BDC}$ = 7.72 mA cm^{-2} at 0.45 V, $I_{Ni\text{-}BDC\text{-}NH2}$ = 14.15 mA cm^{-2} at 0.53 V and $I_{Ni\text{-}BDC\text{-}OH}$ = 2.41 mA cm^{-2} at 0.46 V), noting that bare GCE does not have any catalytic activity towards glucose as there was no Faradaic peak in the CV curve. The CV of Ni-BDC-NH_2 revealed a remarkably higher current response of 1.8- and 5.9-fold higher than Ni-BDC and Ni-BDC-OH, respectively. This can be ascribed to a favourable morphology for Ni-BDC-NH_2 of a micro-sheet structure with multidimensional pores, which facilitate a close interaction between the glucose and active site through pores and channels. Worth noting is the presence of –NH_2 functional group on the BDC linker and its ability to further facilitate the electron transfer to the metal centre of Ni^{2+} in the MOFs structure, as reflected by the profound oxidation peak current for Ni-BDC-NH_2 electrode in the presence of glucose. Moreover, the –NH_2 group in the MOF was also responsible for electrochemical adsorption of glucose molecules.

EIS analysis was examined at a frequency range of 0.01 Hz to 100 kHz to validate the charge transfer behaviour of the modified electrodes. Fig. 2C illustrated the Nyquist plot of bare GCE, Ni-BDC, Ni-BDC-NH_2 and Ni-BDC-OH in 1 mM $[Fe(CN)_6]^{3-/4-}$ with 0.1 M KCl as the supporting electrolyte and 1 mM glucose. It was obvious that the straight line at lower frequencies (post-semicircle) of Ni-BDC-NH_2 was nearly vertical in approaching the imaginary axis (-Z"). This behaviour refers to low ionic diffusion resistance between the electrolyte and the electrode materials. Besides, the semicircle at the high-frequency range indicates the charge transfer resistance (R_{ct}) when electrolyte ions diffused into the electrode through electrode/-electrolyte interface. By referring to the Nyquist plot, the R_{ct} values for the synthesized MOFs were in the order of Ni-BCD-NH_2 (608.7 Ω) < Ni-BDC-OH (757.1 Ω) < Ni-BDC (1371.2 Ω) < bare GCE (2029.7 Ω). The electron transfer rate constant (K_{et}) values, calculated from the R_{ct} values, were determined by equivalent circuit fitting using Eq. (1).

$$K_{et} = \frac{RT}{n^2F^2AC_0R_{ct}} \quad (1)$$

where R is gas constant (8.314 J K^{-1} mol^{-1}), T is temperature in K, n is the number of electrons, F is Faraday's constant (96,485 C mol^{-1}), A is the electrode surface area in cm^2, C is the concentration of redox probe in mol L^{-1} and R_{ct} is the charge transfer resistance in Ω. Using Eq. (1) and the R_{ct} values determined from impedance measurements, the electron transfer rate constant values were calculated and presented in Table 1. Ni-BDC-NH_2 electrode illustrated the fastest electron transfer rate of 5.67 cm s^{-1} due to the presence of the –NH_2 functional group on the BDC, which facilitated electron transfer from BDC-NH_2 to the Ni^{2+} metal centres.

The mechanism of the electrochemical reaction between glucose and the modified electrode was investigated using the CV profiles of glucose (0.1 mM) at various scan rate (10–100 mV) (Fig. 2D–F). Both anodic and cathodic peak currents for all electrodes were proportional

Table 1
Charge transfer resistance (R_{ct}) and electron transfer rate constant (K_{et}) values obtained for bare GCE, Ni-BDC, Ni-BDC-NH_2 and Ni-BDC-OH in 1 mM $[Fe(CN)_6]^{3-/4-}$ electrolyte.

Electrode	R_{ct}/Ω	K_{et}/cm s^{-1}
Bare GCE	2029.7	1.70
Ni-BDC	1371.2	2.52
Ni-BDC-NH_2	757.1	4.56
Ni-BDC-OH	608.7	5.67

to the function of the scan rate. The anodic potential peak (E_{pa}) shifts positively while the cathodic potential peak (E_{pc}) shifts negatively upon increasing the scan rate. Increases in ΔE_p ($E_{pc} - E_{pa}$) with increasing scan rate were due to uncompensated solution resistance (R_u) [16]. During electrochemical measurements, the potential that the instrument records may not be the potential experienced by the solution in the electrolyte due to R_u. This phenomenon is called ohmic drop, in which it increased the peak-to-peak separation in the voltammogram for a redox event. In order to minimize the ohmic drop, electrode should be as small as possible [17]. Among all modified electrodes, Ni-BDC-NH_2 (Fig. 2E) exhibits distinctly higher redox peaks at different scan rate in 1 mM glucose, which was in good agreement with the CV study conducted in Fig. 2B. The linear relationship of peak current against the square root of scan rate ($\nu^{1/2}$) as depicted in inset of Fig. 2D–F ascribed a diffusion-controlled electrochemical process on the electrode surface.

3.3. Electrocatalytic activity of the Ni-BDC-NH_2 electrode towards glucose detection

The electrochemical oxidation of glucose to gluconate by using Ni-BDC-NH_2 electrocatalyst was analysed in mechanistic detail. The objective was to obtain a better understanding on the origin of the oxidative peak of the CV curve for Ni-BDC-NH_2 in the existence of glucose. By referring to the FT-IR analysis of Ni-BDC-NH_2, the activated MOF structures do not contain an open metal site due to the presence of broad O—H stretching vibration, which indicates the presence of coordinated water molecules from the solvent ligand molecules. Therefore, the electrocatalytic oxidation of glucose might not take place at the Ni^{2+} active sites. Inspired by the chemical adsorption mechanism for glucose oxidation proposed by Siyong Gu [18] based on B-*N*-*co*-doped graphene quantum dot (GQD) electrocatalyst and Pasta's group [19] based on Au, Ni-BDC-NH_2 electrode was also found to mimic the same adsorption mechanism. Fig. 3 summarizes the mechanism and the crucial chemical steps involved. Firstly, the glucose molecule was electrochemically adsorbed at the surface of the electrode (specifically at a N site of the Ni-BDC-NH_2 electrocatalyst) by dehydrogenation forming Ni-BDC-NH-glucose (Reaction (1)). Second, the dehydrogenated molecule was transformed to gluconate through direct oxidation, which involves the generation of a hydroxide ion (OH^-) and the elimination of a proton (H^+) (Reaction 2). An alternative path was the oxidation of the dehydrogenated glucose to δ-gluconolactone. The δ-gluconolactone was then transformed to gluconate after reacting with a hydroxide ion (Reaction 3). To the best of our knowledge, this was the first time such a mechanism on the electrocatalytic oxidation of glucose was proposed for a non-enzymatic glucose sensor-based MOF.

Fig. 4A depicted the CVs curves of Ni-BDC-NH_2 electrode in different concentrations of glucose in the potential range 0–0.7 V. The anodic peak of Ni-BDC-NH_2 depicted the shifting in potential to the positive direction (0.53 to 0.59 V) upon increasing glucose concentration in the range from 0.1 to 1.4 mM (inset of Fig. 4A) owing to the superior electrocatalytic oxidation activity of Ni-BDC-NH_2 towards glucose. The corresponding calibration curve of the anodic peak current was linearly dependent (R^2 = 0.9992 at low concentration range and R^2 = 0.9136 at high concentration range) on the concentration of glucose as demonstrated in the Supplementary Information, Fig. S5. To obtain an optimal amperometric current response, applied potentials on the Ni-BDC-NH_2 electrode were varied from 0.45 to 0.60 V in 0.1 M NaOH solution as demonstrated in Fig. 4B. Upon successively dropping 0.1 mM glucose into the electrolyte, the Ni-BDC-NH_2 sensor exhibited a stair-step response under different applied potential. It was apparent that the current response (in the presence of 0.1 mM glucose) increased abruptly when the potential was increased from 0.45 to 0.55 V, and then a small reduction in current was observed when the applied potential was set at 0.6 V. Consequently, 0.55 V was selected as the optimal potential for this non-enzymatic amperometric glucose sensor.

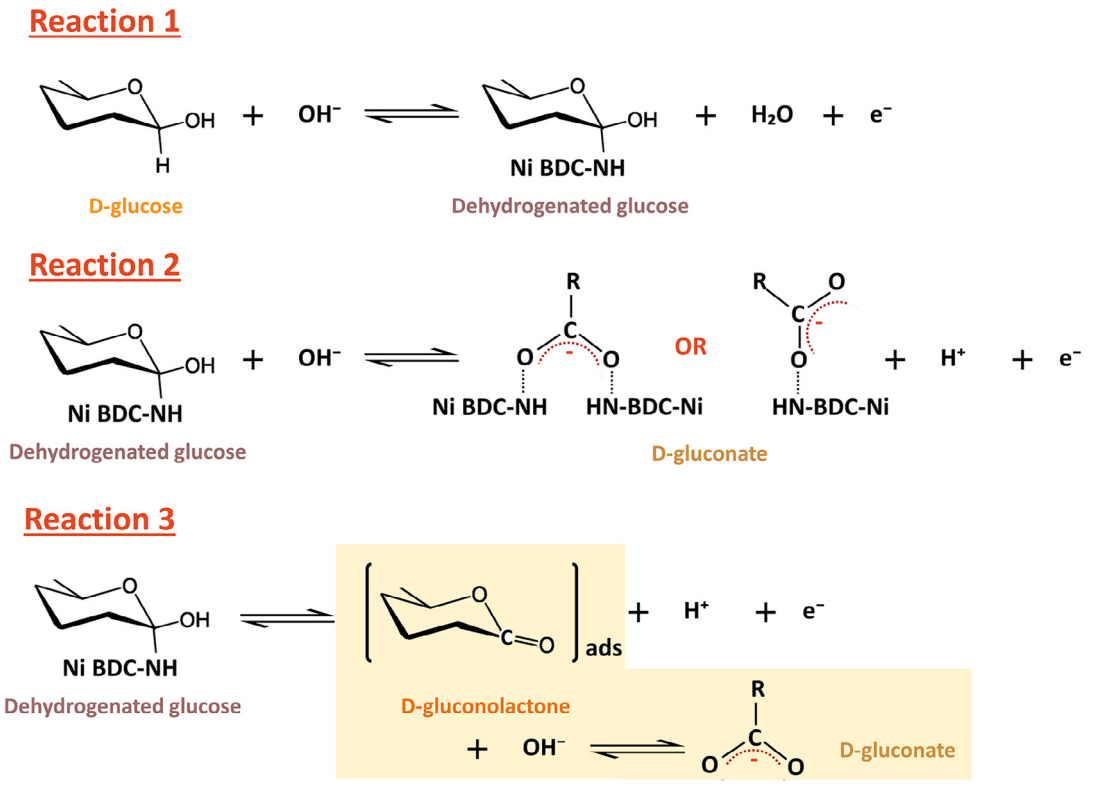

Fig. 3. Proposed mechanism at the Ni-BDC-NH_2 modified electrode towards a non-enzymatic glucose sensor.

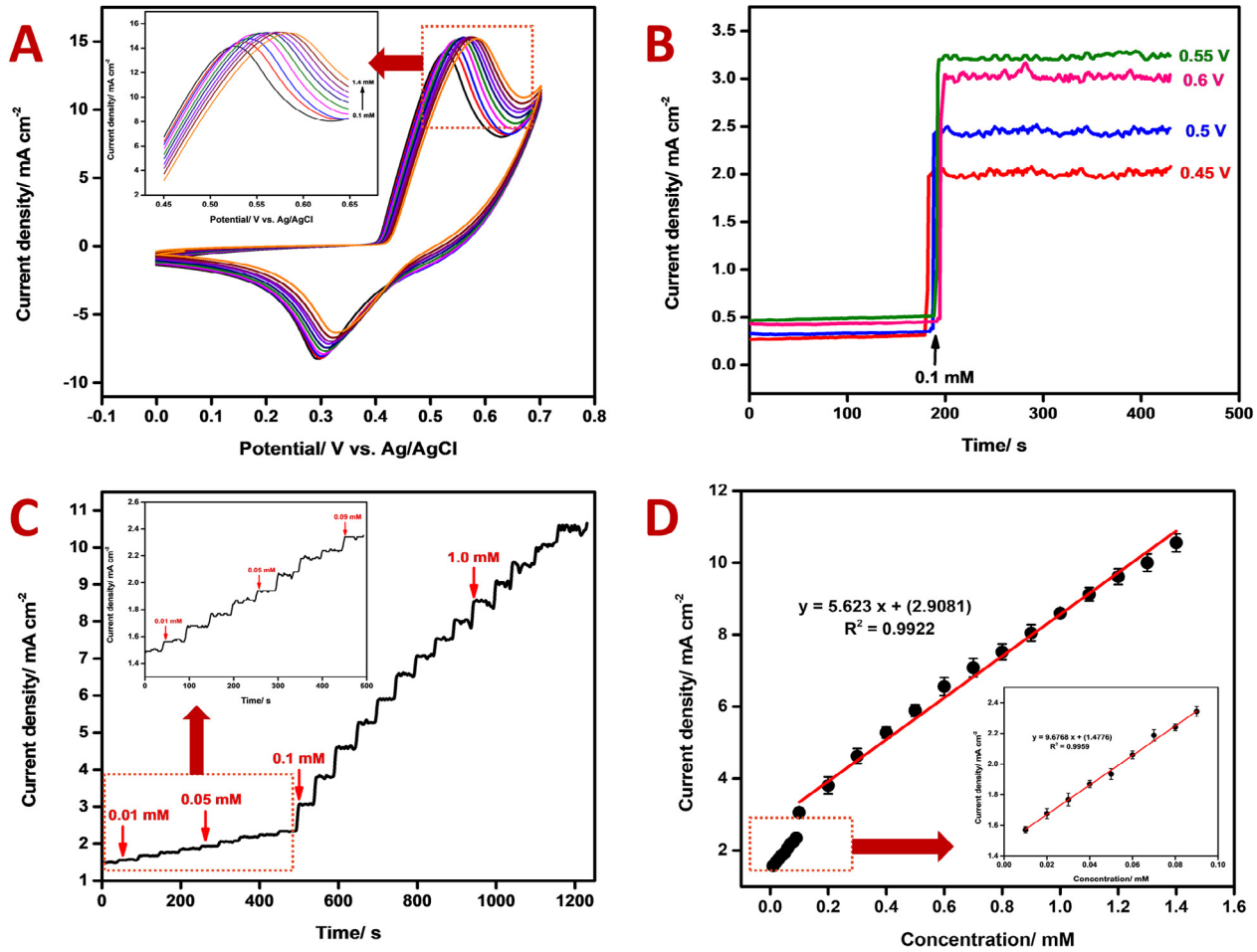

Fig. 4. (A) CV profiles obtained upon addition of various concentrations of glucose from 0.1 to 1.4 mM in 0.1 M NaOH (scan rate: 50 mV s^{-1}). Inset: the magnified oxidation curve of Ni-BDC-NH_2. Amperometric response of Ni-BDC-NH_2 electrode towards successive addition of (B) 0.1 mM glucose at different applied potentials and (C) injection of glucose with different concentrations in 0.1 M NaOH solution at 0.55 V. Inset: amperometric response of the conductive Ni-BDC-NH_2 at low glucose concentrations. (D) The corresponding calibration curve for current vs concentration of glucose. Inset: corresponding calibration curve at low glucose concentrations (n = 3).

The sensitivity and the response time of the Ni-BDC-NH_2 electrode upon addition of various concentrations of glucose were examined by amperometric measurement. Fig. 4C shows the amperometric responses with consecutive step changes of glucose concentration in 0.1 M NaOH solution with constant stirring and an applied potential at 0.55 V. The inset of Fig. 4C shows the amperometric response of lower concentration of glucose from 0.01 to 0.09 mM. Upon successive glucose addition, a stepwise increase in current response was acquired within an average of 5.4 s (Supplementary Information, Fig. S6), which signifies favourable electron mobility assisted the current response due to the conductive Ni-BDC-NH_2 electrode. The response time was evaluated from the beginning at which the glucose was added to the electrolyte until the current slowly increases until it plateaus and becomes stable (Supplementary Information, Fig. S7). The result indicates the fast response time of the conductive Ni-BCD-NH_2/GCE electrode towards glucose detection. Fig. 4D displays the corresponding calibration curve with a linear dependence on the glucose concentration in the range of 0.01 to 1.4 mM attained from the current-time curve. The inset of Fig. 4D displays the magnified standard curve between current and low concentration of glucose (0.01 to 0.09 mM). The calibration curve in the range of 0.01–0.09 mM and 0.1–1.4 mM represents a satisfactory linear relationship with correlation coefficient of 0.9959 and 0.9922, respectively. The detection limit and sensitivity were calculated as 3.82 μM (S/N = 3) and 308 μA mM^{-1} cm^{-2}, respectively. Compared to other electrode materials-based MOFs (Table 2), the conductive Ni-BDC-NH_2 electrode depicted a lower limit of detection and comparable sensitivity. Based on Table 2, other works report a lower detection limit than our work, but those electrodes suffered from poor sensitivity, which may cause inaccuracies of the data when applied in real glucose devices. Blood sugar concentration of between 3.3 and 7.8 mM is considered to be healthy [20]. Herein, our detection limit for Ni-BDC-NH_2 electrode was within the range for healthy blood sugar level. Hence, these results verify that Ni-BDC-NH_2 is a promising and potential material for non-enzymatic glucose detection for clinical diagnostics.

3.4. Analytical performance of the Ni-BDC-NH_2 glucose sensor electrode

For efficient sensing performance, the active materials for non-enzymatic electrochemical sensor devices must be robust in differentiating between the target molecule and the interfering molecules in the test sample. The relatively higher applied potential to oxidize glucose in conventional amperometric sensors can also oxidize other compounds existing in the sample, thus resulting in an overestimated amperometric current value. Consequentially, it may lead to life-threatening complications, such as hyperglycaemia and hypoglycaemia, which may cause coma or even death [27]. Some compounds found in blood can interfere with the glucose detection as they are

Table 2
Comparison of amperometric non-enzymatic glucose sensors using different MOFs-based materials.

Electrode materials	Sensitivity ($\mu A\ mM^{-1}\ cm^{-2}$)	Linear range (mM)	Detection limit (μM)	Ref.
Ni-BDC MOF	635.9	0.01–0.8	6.68	[21]
Cu_2O@ZIF-67	181.34	0.01–16.3	6.5	[22]
ZIF-N_2	227	0.1–1.1	5.69	[23]
Ni(TPA)-SWCNT	–	0.2–4.4	4.6	[14]
Cu-MOF	89	0.1–3.5	2.4	[24]
Ag@TiO_2@ZIF-67	0.788	0.048–1	0.99	[2]
Ag@ZIF-67	0.379	0.002–1	0.66	[25]
Cu nanospheres@porous carbon/3D-KSCs	28.67	0.00015–5.62	0.48	[26]
Ni-BDC-NH_2	308	0.01–1.4	3.82	This work

ZIF – zeolitic imidazolate framework; TPA – terephthalic acid; SWCNT – single-walled carbon nanotubes; 3D-KSCs – three-dimensional kenaf stem-derived macroporous carbon.

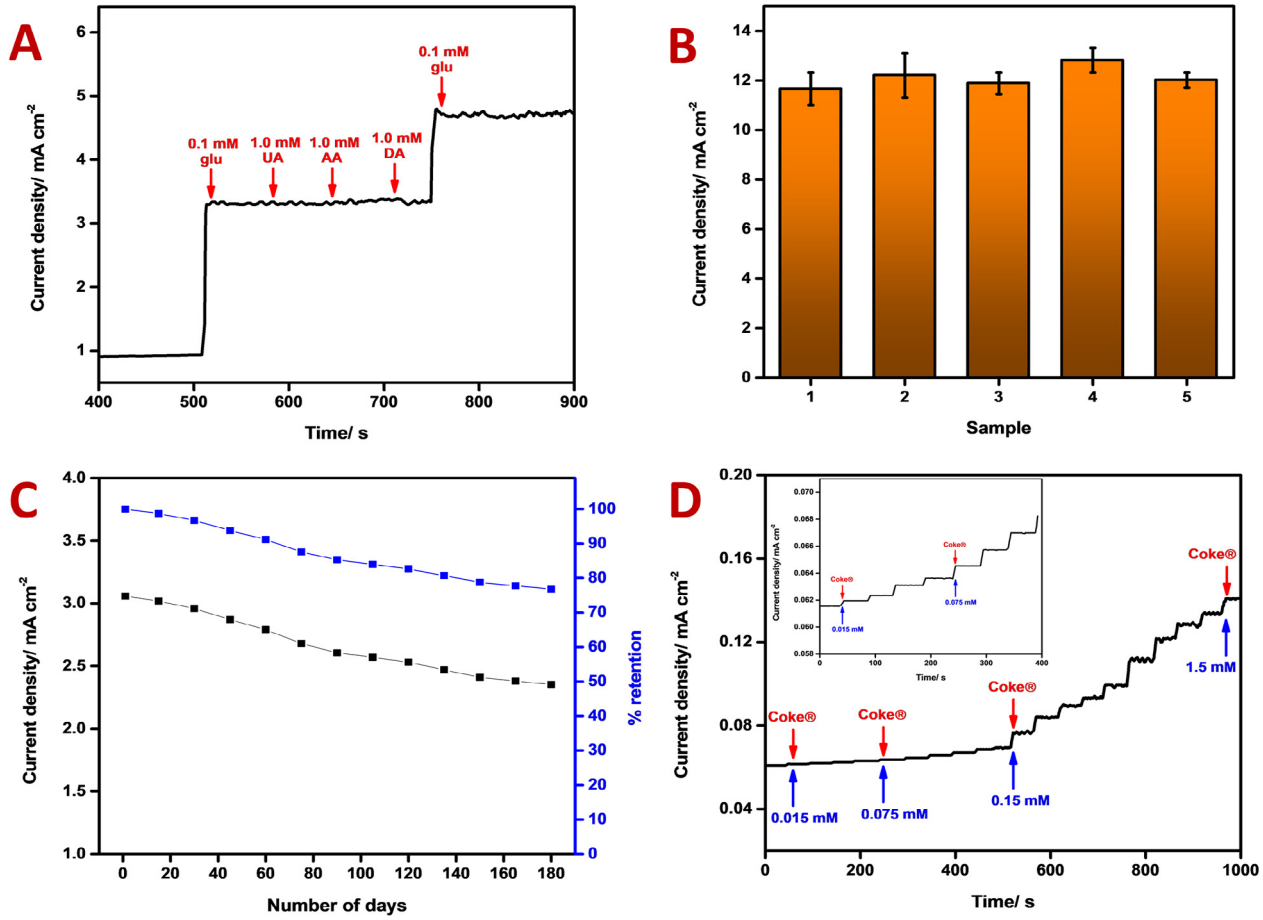

Fig. 5. (A) Amperometric response of Ni-BDC-NH_2 electrode toward the addition of 0.1 mM glucose and other interference compounds. (B) Amperometric response of five independent electrodes in 0.1 M NaOH containing 0.1 mM glucose at working potential of 0.55 V. (C) Long-term stability of the glucose sensor over 180 days. (D) Amperometric responses of Ni-BDC-NH_2 electrode on the successive addition of soft drink (Coca-Cola) Inset: amperometric response of the conductive Ni-BDC-NH_2 at low glucose concentrations.

strong reducing agents similar to glucose, which subsequently can oxidize at the selected potential. Common interferents found in blood are uric acid (UA), ascorbic acid (AA) and dopamine (DA). Therefore, an experiment was designed to investigate the selectivity of the Ni-BDC-NH_2 electrode towards glucose oxidation with the results being depicted in Fig. 5A. It was observed that when 0.1 mM of glucose was successively added into 0.1 M NaOH pH, a profound enhancement in current was seen. However, after the introduction of 10 times higher concentration (1 mM) of the interference compounds, a negligible amperometric response appeared, but the current response increased sharply again with another addition of 0.1 mM of glucose. This interesting outcome suggests that the molecular sieve effect of the Ni-BDC-NH_2 MOF was crucial for good selectivity in glucose detection based on the non-enzymatic approach. The molecular sizes of the interfering species (DA = 8.55, AA = 7.15, and UA = 7.11 Å) were larger than that of glucose (6.96 Å) [5]. This led to a more sluggish diffusion of the

interfering species into the MOF tunnels that helped the Ni-BDC-NH_2 electrode to simulate enzymatic selectivity to some extent for glucose sensing.

The reproducibility of the Ni-BDC-NH_2 modified GCE sensor was investigated by measuring the current response to 0.1 mM glucose using five independent electrodes under the same condition. As observed in Fig. 5B, the introduction of similar concentration of glucose resulted in almost equal current density with relative standard deviation (RSD) of 3.6 %, confirming a good reproducibility of Ni-BDC-NH_2 electrode. The long-term stability of glucose sensor was a critical factor in practical sensor application. The experiment was assessed by considering the amperometric response in 0.1 M NaOH containing 0.1 mM glucose. The Ni-BDC-NH_2 electrode was stored in a clean container at atmospheric condition and the current response was tested every 15 d. This sensor retains about 77 % of its initial current density after 180 d of storage as illustrated in Fig. 5C. In addition, the RSD was only 9.3 % which portrays the reliability of Ni-BDC-NH_2 in the application of non-enzymatic glucose sensing. To verify the practicality of the modified sensor in sample analysis, Ni-BDC-NH_2 was employed to detect the concentration of glucose in soft drink (Coca-Cola or 'Coke'). Fig. 5D displays the amperometric curve of Ni-BDC-NH_2 with continuous addition of diluted soft drink (0.5 % *v*/*v*). The results illustrated that the current densities increase with increasing glucose concentration ranging from 0.015 to 1.5 mM, indicating its potential application of glucose detection.

4. Conclusion

Ni-based MOF sensors were designed using a facile solvothermal approach by reacting Ni^{2+} with BDC or a functionalized BDC linker (BDC-NH_2 and H_2BDC-OH). The physicochemical features of the as-prepared MOFs were characterized by FE-SEM, EDX, XRD and FTIR. The XRD study has verified that there are no notable changes in the structure containing the parent linker (BDC) when comparing to the MOFs containing functionalized linkers (BDC-NH_2 and H_2BDC-OH). The morphology of Ni-BDC-NH_2 displayed a hierarchical multi-layered sheet-like structure with multidimensional pores. This architecture has accelerated the diffusion velocity of the glucose molecules, thus beneficial for the enhancement of electrochemical performance. Ni-BDC-NH_2/GCE exhibited an excellent electrocatalytic behaviour towards oxidation of glucose compared to other electrodes in an alkaline media (pH = 13), hence this electrode was employed for further practical analysis on glucose sensor. As an electrochemical non-enzymatic glucose sensor, Ni-BDC-NH_2 shows a comparable fast response time within 5.4 s, low detection limit of 3.82 μM (S/N = 3), and high sensitivity of 308 μA mM^{-1} cm^{-2}, accompanied by exceptional reproducibility and long-term stability of 76.8 % retention after 180 days. The presence of $–NH_2$ functional group in the linker molecules not only facilitated electron transfer, but also was responsible for electrochemical adsorption of glucose molecules, which resulted in remarkable sensing performance. Worth noting that the molecular sieve effect of the tunnels in the MOF enabled the selective diffusion of glucose during an interference study and this made the sensors exhibit impressive selectivity even when the concentrations of the interfering species reached 10-fold higher than glucose. Ultimately, the proposed glucose sensor materials not only provide remarkable performance in glucose determination, but also demonstrates an exciting path for fabrication, development and utilization of a conductive MOF.

CRediT authorship contribution statement

A.D. Daud: Methodology, Investigation, Writing – original draft. **H.N. Lim:** Supervision, Conceptualization, Funding acquisition. **I. Ibrahim:** Methodology, Writing – review & editing, Visualization, Investigation. **N.A. Endot:** Supervision, Validation. **N.S.K. Gowthaman:** Validation. **Z.T. Jiang:** Validation. **Kyle E. Cordova:** Conceptualization, Data curation, Funding acquisition.

Data availability

The data that has been used is confidential.

Declaration of Competing Interest

The authors declare that they have no known competing financial interests or personal relationships that could have appeared to influence the work reported in this paper.

Acknowledgements

This work was supported by the Fundamental Research Grant Scheme (FRGS) FRGS/1/2021/STG05/UPM/01/1 from the Ministry of Higher Education of Malaysia (MOHE). K.E.C. is grateful to support provided by MISTI Global Seed Funds and the MIT-Jordan Abdul Hameed Shoman Foundation Seed Fund, United States (No. 0000000093) as well as the Jordan Ministry of Higher Education and Scientific Research, Jordan (BAS/1/6/2020).

Appendix A. Supplementary data

Supplementary data to this article can be found online at https://doi.org/10.1016/j.jelechem.2022.116676.

References

[1] A. Afroz, M.J. Alramadan, M.N. Hossain, L. Romero, K. Alam, D.J. Magliano, B. Billah, Cost-of-illness of type 2 diabetes mellitus in low and lower-middle income countries: a systematic review, BMC Health Services Res. 18 (2018) 1–10.
[2] D. Arif, Z. Hussain, M. Sohail, M.A. Liaqat, M.A. Khan, T. Noor, A non-enzymatic electrochemical sensor for glucose detection based on Ag@TiO_2@metal-organic framework (ZIF-67) nanocomposite, Front. Chem. 8 (2020) 573510.
[3] X. Xuan, M. Qian, L. Pan, T. Lu, L.u. Han, H. Yu, L. Wan, Y. Niu, S. Gong, A longitudinally expanded Ni-based metal–organic framework with enhanced double nickel cation catalysis reaction channels for a non-enzymatic sweat glucose biosensor, J. Mater. Chem. B 8 (39) (2020) 9094–9109.
[4] H. Jia, N. Shang, Y. Feng, H. Ye, J. Zhao, H. Wang, C. Wang, Y. Zhang, Facile preparation of Ni nanoparticle embedded on mesoporous carbon nanorods for non-enzymatic glucose detection, Journal of Colloid, Interface Sci. 583 (2021) 310–320.
[5] L.i. Zhang, X. Ma, H. Liang, H. Lin, G. Zhao, A non-enzymatic glucose sensor with enhanced anti-interference ability based on a MIL-53 (NiFe) metal–organic framework, J. Mater. Chem. B 7 (44) (2019) 7006–7013.
[6] L. Wang, N. Deng, G. Wang, J. Ju, B. Cheng, W. Kang, Constructing amino-functionalized flower-like metal–organic framework nanofibers in sulfonated poly (ether sulfone) proton exchange membrane for simultaneously enhancing interface compatibility and proton conduction, ACS Appl. Mater. Interfaces 11 (43) (2019) 39979–39990.
[7] Y. Qiao, Q. Liu, S. Lu, G. Chen, S. Gao, W. Lu, X. Sun, High-performance non-enzymatic glucose detection: using a conductive Ni-MOF as an electrocatalyst, J. Mater. Chem. B 8 (2020) 5411–5415.
[8] A. Carton, A. Mesbah, T. Mazet, F. Porcher, M. François, Ab initio crystal structure of nickel (II) hydroxy-terephthalate by synchrotron powder diffraction and magnetic study, Solid State Sci. 9 (6) (2007) 465–471.
[9] Y. Zhao, H. Wu, T.J. Emge, Q. Gong, N. Nijem, Y.J. Chabal, L. Kong, D.C. Langreth, H. Liu, H. Zeng, J. Li, Enhancing gas adsorption and separation capacity through ligand functionalization of microporous metal–organic framework structures, Chemistry–A Eur. J. 17 (18) (2011) 5101–5109.
[10] P. Thangasamy, S. Shanmuganathan, V. Subramanian, A NiCo-MOF nanosheet array based electrocatalyst for the oxygen evolution reaction, Nanoscale Adv. 2 (5) (2020) 2073–2079.
[11] B. Iqbal, M. Saleem, S.N. Arshad, J. Rashid, N. Hussain, M. Zaheer, One-pot synthesis of heterobimetallic metal–organic frameworks (MOFs) for multifunctional catalysis, Chemistry–A Eur. J. 25 (44) (2019) 10490–10498.
[12] A.J. Rieth, K.M. Hunter, M. Dincă, F. Paesani, Hydrogen bonding structure of confined water templated by a metal-organic framework with open metal sites, Nat. Commun. 10 (2019) 1–7.
[13] Y. Nian, L. Luo, W. Zhu, C. Yang, L. Zhang, M. Li, W. Zhang, J. Wang, Does intrinsic photocontrollable oxidase-mimicking activity of 2-aminoterephthalic acid dominate the activity of metal− organic framework?, Inorgan Chem. Front. 8 (2021) 3482–3490.

[14] F. Wang, X. Chen, L. Chen, J. Yang, Q. Wang, High-performance non-enzymatic glucose sensor by hierarchical flower-like nickel (II)-based MOF/carbon nanotubes composite, Mater. Sci. Eng.: C 96 (2019) 41–50.
[15] Y. Li, M. Xie, X. Zhang, Q. Liu, D. Lin, C. Xu, F. Xie, X. Sun, Co-MOF nanosheet array: a high-performance electrochemical sensor for non-enzymatic glucose detection, Sens. Actuators B Chem. 278 (2019) 126–132.
[16] N. Elgrishi, K.J. Rountree, B.D. McCarthy, E.S. Rountree, T.T. Eisenhart, J.L. Dempsey, A practical beginner's guide to cyclic voltammetry, J. Chem. Educ. 95 (2) (2018) 197–206.
[17] K.J. Aoki, J. Chen, Y. Liu, B. Jia, Peak potential shift of fast cyclic voltammograms owing to capacitance of redox reactions, J. Electroanal. Chem. 856 (2020) 113609.
[18] S. Gu, C.T. Hsieh, C.P. Kao, C.C. Fu, Y. Ashraf Gandomi, R.S. Juang, K.D. Kihm, Electrocatalytic oxidation of glucose on boron and nitrogen codoped graphene quantum dot electrodes in alkali media, Catalysts 11 (2021) 101.
[19] M. Pasta, F. La Mantia, Y.i. Cui, Mechanism of glucose electrochemical oxidation on gold surface, Electrochim. Acta 55 (20) (2010) 5561–5568.
[20] J.J. García-Guzmán, C. Pérez-Ràfols, M. Cuartero, G.A. Crespo, Microneedle based electrochemical (bio) sensing: towards decentralized and continuous health status monitoring, Trends Anal. Chem. 135 (2021) 116148.
[21] G. Gumilar, Y.V. Kaneti, J. Henzie, S. Chatterjee, J. Na, B. Yuliarto, N. Nugraha, A. Patah, A. Bhaumik, Y. Yamauchi, General synthesis of hierarchical sheet/plate-like M-BDC (M = Cu, Mn, Ni, and Zr) metal–organic frameworks for electrochemical non-enzymatic glucose sensing, Chem. Sci. 11 (14) (2020) 3644–3655.
[22] N. Yang, K. Guo, Y. Zhang, C. Xu, Engineering the valence state of ZIF-67 by Cu_2O for efficient nonenzymatic glucose detection, J. Mater. Chem. B 8 (14) (2020) 2856–2861.
[23] L. Shi, Y. Li, X. Cai, H. Zhao, M. Lan, ZIF-67 derived cobalt-based nanomaterials for electrocatalysis and nonenzymatic detection of glucose: difference between the calcination atmosphere of nitrogen and air, J. Electroanal. Chem. 799 (2017) 512–518.
[24] Y. Sun, Y. Li, N. Wang, Q.Q. Xu, L. Xu, M. Lin, Copper-based metal-organic framework for non-enzymatic electrochemical detection of glucose, Electroanalysis 30 (3) (2018) 474–478.
[25] W. Meng, Y. Wen, L. Dai, Z. He, L. Wang, A novel electrochemical sensor for glucose detection based on Ag@ ZIF-67 nanocomposite, Sens. Actuators B Chem. 260 (2018) 852–860.
[26] Y. Xie, Y. Song, Y. Zhang, L. Xu, L. Miao, C. Peng, L. Wang, Cu metal-organic framework-derived Cu nanospheres@porous carbon/macroporous carbon for electrochemical sensing glucose, J. Alloys Compd. 757 (2018) 105–111.
[27] B.G. Amin, J. Masud, M. Nath, A non-enzymatic glucose sensor based on a $CoNi_2Se_4$/rGO nanocomposite with ultrahigh sensitivity at low working potential, J. Mater. Chem. B 7 (14) (2019) 2338–2348.